

Article

Catalysts Based on Iron Oxides for Wastewater Purification from Phenolic Compounds: Synthesis, Physicochemical Analysis, Determination of Catalytic Activity

Binara T. Dossumova¹, Larissa R. Sassykova^{2,*}, Tatyana V. Shakiyeva¹, Dinara Mukhtaly¹,
Aigul A. Batyrbayeva² and Madina A. Kozhaisakova³

¹ Al-Farabi Kazakh National University, Almaty 050040, Kazakhstan; dossumova63@mail.ru (B.T.D.); shakievatatyana@mail.ru (T.V.S.); dinara.muktaly@mail.ru (D.M.)

² Faculty of Chemistry and Chemical Technology, Al-Farabi Kazakh National University, Almaty 050040, Kazakhstan; batyrbaeva_aigul@mail.ru

³ Department of Chemistry, Chemical Technology and Ecology, Almaty Technological University, Almaty 050012, Kazakhstan; madina.69@mail.ru

* Correspondence: larissa.rav@mail.ru

Abstract: In this work, the synthesis of magnetite nanoparticles and catalysts based on it stabilized with silicon and aluminum oxides was carried out. It is revealed that the stabilization of the magnetite surface by using aluminum and silicon oxides leads to a decrease in the size of magnetite nanocrystals in nanocomposites (particle diameter less than ~10 nm). The catalytic activity of the obtained catalysts was evaluated during the oxidation reaction of phenol, pyrocatechin and cresol with oxygen. It is well known that phenolic compounds are among the most dangerous water pollutants. The effect of phenol concentration and the effect of temperature (303–333 K) on the rate of oxidation of phenol to Fe₃O₄/SiO₂ has been studied. It has been determined that the dependence of the oxidation rate of phenol on the initial concentration of phenol in solution is described by a first-order equation. At temperatures of 303–313 K, incomplete absorption of the calculated amount of oxygen is observed, and the analysis data indicate the non-selective oxidation of phenol. Intermediate products, such as catechin, hydroquinone, formic acid, oxidation products, were found. The results of UV and IR spectroscopy showed that catalysts based on magnetite Fe₃O₄ are effective in the oxidation of phenol with oxygen. In the UV spectrum of the product in the wavelength range 190–1100 nm, there is an absorption band at a wavelength of 240–245 nm and a weak band at 430 nm, which is characteristic of benzoquinone. In the IR spectrum of the product, absorption bands were detected in the region of 1644 cm⁻¹, which is characteristic of the oscillations of the C=O bonds of the carbonyl group of benzoquinone. The peaks also found at 1353 cm⁻¹ and 1229 cm⁻¹ may be due to vibrations of the C-H and C-C bonds of the quinone ring. It was found that among the synthesized catalysts, the Fe₃O₄/SiO₂ catalyst demonstrated the greatest activity in the reaction of liquid-phase oxidation of phenol.

Keywords: catalysts; magnetite; aluminium oxide; silicon oxide; oxygen; oxidation; phenol; composite catalysts



Citation: Dossumova, B.T.; Sassykova, L.R.; Shakiyeva, T.V.; Mukhtaly, D.; Batyrbayeva, A.A.; Kozhaisakova, M.A. Catalysts Based on Iron Oxides for Wastewater Purification from Phenolic Compounds: Synthesis, Physicochemical Analysis, Determination of Catalytic Activity. *ChemEngineering* **2024**, *8*, 8. <https://doi.org/10.3390/chemengineering8010008>

Academic Editor: Nicolas Roche

Received: 27 September 2023

Revised: 26 November 2023

Accepted: 8 December 2023

Published: 1 January 2024



Copyright: © 2024 by the authors. Licensee MDPI, Basel, Switzerland. This article is an open access article distributed under the terms and conditions of the Creative Commons Attribution (CC BY) license (<https://creativecommons.org/licenses/by/4.0/>).

1. Introduction

The main share of pollution of water bodies comes from emissions of industrial untreated wastewater from industrial, agricultural, storm water and municipal enterprises [1–12]. One of the urgent problems of environmental protection is the neutralization of wastewater from dissolved organic pollutants. This problem is particularly pressing in the case of phenol-containing wastewater. Phenolic compounds are among the most dangerous water pollutants. Waters with impurities of phenols are called “phenolic”. Phenol is a highly toxic compound that has an extremely adverse effect on living organisms

not only by its toxicity but also by a significant change in the regime of biogenic elements and dissolved gases (oxygen and carbon dioxide). A large amount of phenol is discharged into reservoirs from oil and coke chemical, pulp and paper, shale processing, coal enterprises, and processes for obtaining and processing phenols. According to the World Health Organization, phenol is a highly toxic substance, and in terms of the level of pollution of the hydrosphere, it is in third place after petroleum products and heavy metals. Phenol is an industrial pollutant, quite toxic to animals and humans, and destructive to many microorganisms; therefore, industrial wastewater with a high content of phenol is poorly amenable to biological treatment. Getting into running waters and being absorbed into soils, phenol-containing compounds have a negative impact on natural biocenosis and can be the initiator of many environmental problems [13–19].

Available data in the literature indicate that almost all organic components of wastewater can be oxidized. To reduce the concentration of harmful substances in industrial wastewater, many methods are applicable, among which catalytic purification is one of the most effective methods [20–31]. To accelerate oxidation, scientists have proposed a variety of catalysts, and reactions of catalytic oxidation of organic compounds are practically irreversible and, in the presence of suitable catalysts, can completely transform toxic substances into harmless products, such as carbon dioxide and water. In recent years, oxidative degradation in the presence of solid catalysts has been used to clean wastewater contaminated with organic compounds, among which materials containing iron ions fixed on various carriers (zeolite, coals, aluminosilicates, and clays) are promising. Heterogeneous catalytic oxidation of organic compounds in aqueous solutions makes it possible to avoid secondary contamination of wastewater with iron ions and to carry out destruction with the formation of non-toxic products [29–44]. Despite the large number of developments for the purification of industrial waste from phenols, this problem cannot be considered solved. This is due to the different chemical composition and conditions for the formation of contaminants, the difficulty of following the cleaning process, the high economic costs associated with the use of scarce reagents, their subsequent regeneration and the need to dispose of the resulting toxic waste. Therefore, it is quite difficult to ensure highly effective purification from phenol compounds in most enterprises. The search for catalysts for the oxidation of organic substances in aqueous solutions is an urgent task [40–55].

Over the past decades, nanotechnology has become a very popular area of research. This increased interest is due to the fact that the synthesized nanoparticles have unique physicochemical properties (optical, electrical, magnetic) and mechanical properties. The reason lies in the effect of the transition from micro-dimensions to nano-dimensions, wherein the ratio of surface to volume, that is, the proportion of surface atoms in relation to volumetric units, increases [32,33,38–43,56]. The most noticeable in such cases are changes in the magnetic properties of nanoparticles compared to micro-sized materials. In general, the magnetic behavior of nanoparticles is determined by important physical characteristics, such as particle size, crystal lattice type, and particle morphology. The synthesis of magnetic nanoparticles is a promising area of research. To date, magnetic nanoparticles of various compositions and shapes have been synthesized, containing iron oxides (magnetite (Fe_3O_4) and maghemite ($-\text{Fe}_2\text{O}_3$)), as well as pure metals or alloys. Magnetite-based nanomaterials are widely used as part of composite systems in medicine, biotechnology and engineering. In particular, catalysts based on nanosized magnetite have fast adsorption–desorption kinetics and high chemical activity [32–35,37,38,47–52,56–61]. Due to its excellent physicochemical properties, iron oxide (Fe_3O_4) has attracted much attention in recent years. So, the most widely used nanoparticles are those based on iron oxides since, despite their weaker magnetic properties compared to metal nanoparticles, they are more resistant to oxidation, less toxic, and have a wide range of functionalization possibilities. Common modifications of iron oxides are hematite, maghemite and magnetite. Analyzing the magnetic and toxicological properties of nanoparticles based on iron oxides, one can notice fairly effective magnetic characteristics and lower toxicity compared to similar nanoparticles based on nickel, cobalt and other metals.

The aim of this work is to prepare catalysts based on magnetite Fe_3O_4 , study them by using physicochemical research methods, and determine their effectiveness in the catalytic oxidation of phenol, and pyrocatechol and cresol with oxygen.

2. Materials and Methods

The objects of study in this work are nanocrystalline magnetite and magnetite-based composites stabilized by oxides of silicon and aluminum. The synthesis of magnetite with a nanocrystalline structure was described by us in our previous articles [51,52]. To obtain magnetite, we used the reaction of rapid precipitation in an excess of an aqueous solution of ammonia of a mixture of ferrous and ferric salts in an alkaline medium. The resulting magnetic fluids were used to fabricate $\text{Fe}_3\text{O}_4/\text{SiO}_2$ and $\text{Fe}_3\text{O}_4/\text{Al}_2\text{O}_3$ composites.

Mössbauer spectroscopy was used for magnetic structure studies and phase analysis in this study. Mössbauer spectroscopy was performed on an MS-1104 spectrometer. All samples were calibrated for α -Fe. The source of γ -quanta was Co^{57} . The Mössbauer spectra were set at room temperature.

Powder diffraction patterns were recorded on a Bruker D8 Advance ECO X-ray diffractometer (Bruker GmbH, Mannheim, Germany). The diffraction patterns were measured in the Bragg–Brentano geometry in the angle range $2\theta = 15\text{--}100^\circ$. All measurements were carried out under normal conditions. Profex 5.0.2 software was used for qualitative and quantitative analysis of diffractograms. Quantitative analysis was carried out in the program according to the Rietveld method with the criterion of the minimum value of the root-mean-square deviation χ^2 . Qualitative analysis was performed based on the results of energy-dispersive analysis of the scanning electron microscopy (SEM). The average size of magnetite crystallites was determined using X-ray diffraction analysis.

SEM micrographs were registered on a Phenom Pro X microscope (Thermo Fisher Scientific, Waltham, MA, USA). The accelerating voltage during shooting was 15 kV. Before measurements, the powder samples were attached to graphite adhesive tape, followed by the deposition of a nanometer layer of gold via the vacuum deposition method. For elemental analysis and mapping of elements, the X-ray energy-dispersive analysis method was used, which was also performed using a Phenom Pro X microscope.

The IR spectra were recorded and processed on a VERTEX 70 IR Fourier spectrometer in the frequency range from 4000 to 500 cm^{-1} and using a PIKE MIRacle ATR single frustrated internal total reflection (ATR) attachment with a germanium crystal. The results were processed using the OPUS 7.2.139.1294 software.

In this work, studies were carried out on the oxidation of phenol, pyrocatechol and cresol with oxygen as the most typical environmental pollutants.

The oxidation reactions of phenol, pyrocatechol and cresol with oxygen were carried out in a non-flowing glass gradient-free thermostated duck-type reactor equipped with a potentiometric device [51,52]. The kinetic regime was ensured by intense shaking of the reactor (300–400 vibrations per minute); the volume of the liquid phase was no more than 40 cm^3 , with a total reactor volume of 180 cm^3 . The oxidation reaction was examined at $T = 343\text{ K}$, $P_{\text{atm}} = 93.7\text{ kPa}$, $\text{pH} = 5\text{--}6$. The components of the system were added in the following order: the catalyst was loaded into the reactor, then the phenol (or pyrocatechol or cresol) solution was poured. After that, a specified oxygen atmosphere was created in the reactor. The reactor was shaken until a constant volume of the gas phase was established (within the experimental error). The temperature was maintained with an accuracy of 0.5 $^\circ\text{C}$ using a thermostat. When the rate of oxygen absorption became below 0.1 mL/min, the reaction was considered complete; the solution was drained from the reactor and analyzed. The reaction rate was determined by the amount of oxygen absorbed in a thermostated burette connected to the reactor.

A direct method for measuring the absorption spectrum of phenol can be used to determine phenol in water. The sensitivity of the method for the least sensitive absorption band during measurement allows the determination of phenols in water. In this regard,

the UV absorption spectra of an aqueous solution of the starting phenol and the reaction product were recorded.

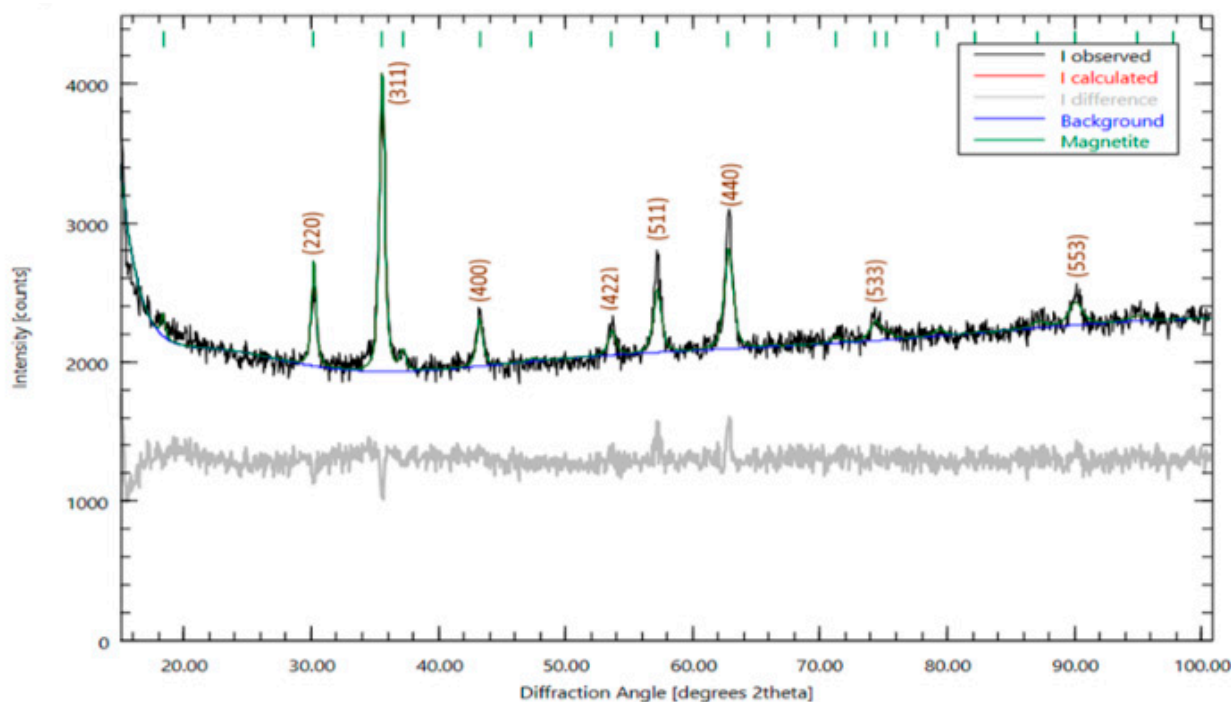
The absorption spectra were measured using a SHIMADZU UV-1240 spectrophotometer, which is a single-beam instrument. The wavelength can vary in the range from 190 to 1100 nm.

3. Results

3.1. Catalysts Characterization

Figure 1 shows the X-ray diffraction pattern of magnetite and composite catalysts $\text{Fe}_3\text{O}_4/\text{SiO}_2$, $\text{Fe}_3\text{O}_4/\text{Al}_2\text{O}_3$. The X-ray diffraction pattern of the synthesized magnetite nanoparticles is in good agreement with the literature data for magnetite. Thus, the diffraction patterns of magnetite and nanocomposites (Figure 1) show peaks at $2\theta = 35.6$; 43.3 ; 53.7 ; 57.2 ; 62.9° , which correspond to the crystalline phase of magnetite Fe_3O_4 and to the lattice planes (311), (400), (422), (511), and (440), respectively, characteristic of magnetite, indicating its crystal structure. The results of X-ray diffraction analysis of the obtained composites demonstrated the presence of a spinel phase with space group $\text{Fd}\bar{3}\text{m}$ and lattice parameter $a = 0.8386$ nm. The average size of magnetite crystallites, calculated by using the Debye–Scherrer formula, is 16–20 nm. Magnetite is the only crystalline phase present in the sample.

For samples of magnetite stabilized by SiO_2 and Al_2O_3 , in addition to the crystalline phase of magnetite, there are SiO_2 , quartz and $\alpha\text{-Al}_2\text{O}_3$ phases, respectively. At 2θ values, peaks of 26.6° were found, characteristic of the crystal lattice of SiO_2 corresponding to (111) and diffraction reflections characteristic of reflections of Fe_3O_4 nanoparticles (Figure 1c). The form of the diffraction pattern indicates the presence of silica in the nanocomposite in the crystalline and amorphous state. The $\text{Fe}_3\text{O}_4/\text{Al}_2\text{O}_3$ diffraction patterns at 2θ values (Figure 1b) show peaks characteristic of the $\alpha\text{-Al}_2\text{O}_3$ crystal lattice. The average size of crystallites for $\text{Fe}_3\text{O}_4/\text{SiO}_2$ and $\text{Fe}_3\text{O}_4/\text{Al}_2\text{O}_3$, calculated by using the Debye–Scherrer formula, is 9–10 nm and 8–10 nm, respectively.



(a)

Figure 1. Cont.

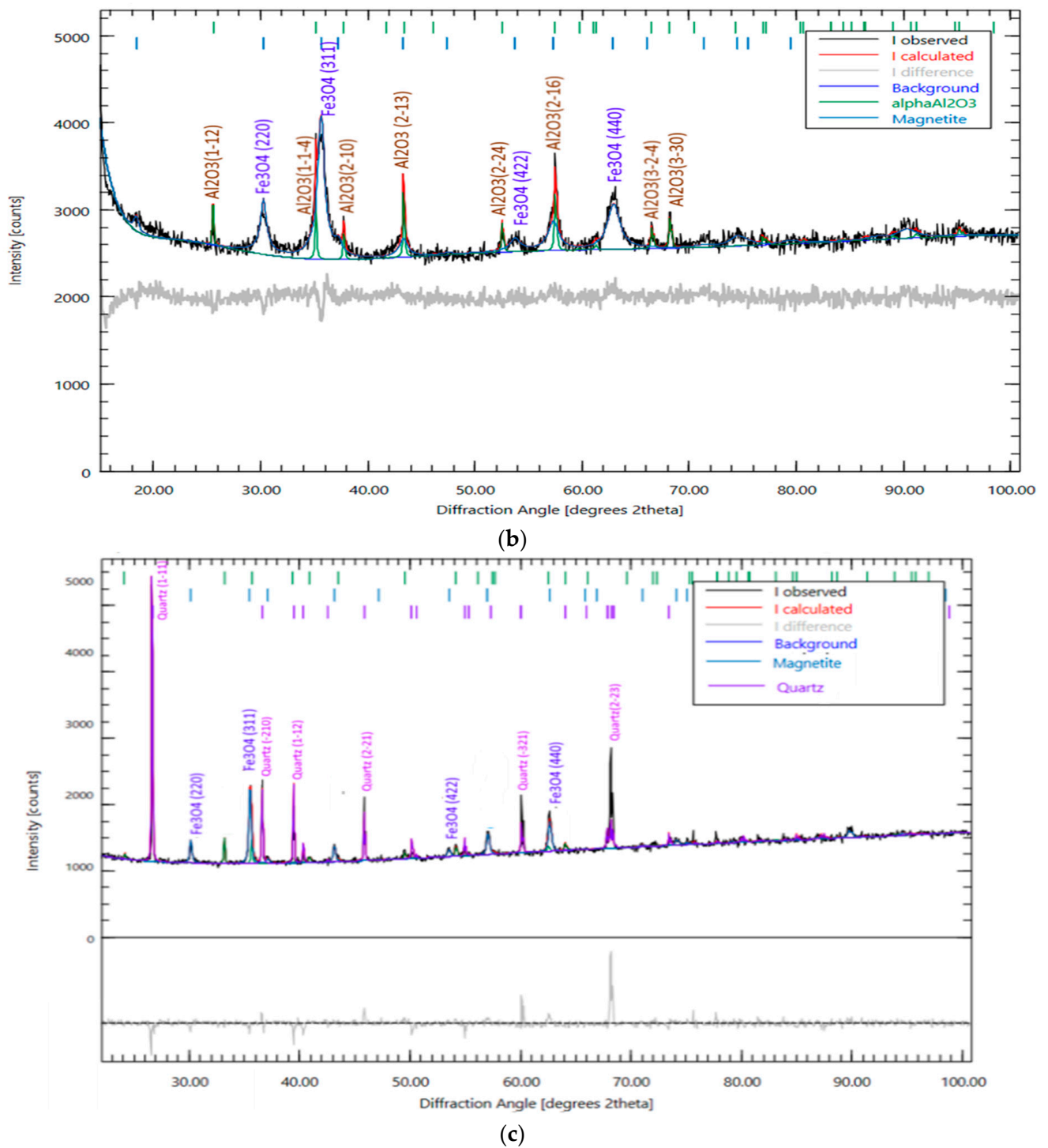


Figure 1. X-ray diffraction patterns of magnetite Fe_3O_4 (a), Fe_3O_4 stabilized Al_2O_3 (b) and Fe_3O_4 stabilized SiO_2 (c).

The size distribution histogram of magnetite particles is shown in Figure 2.

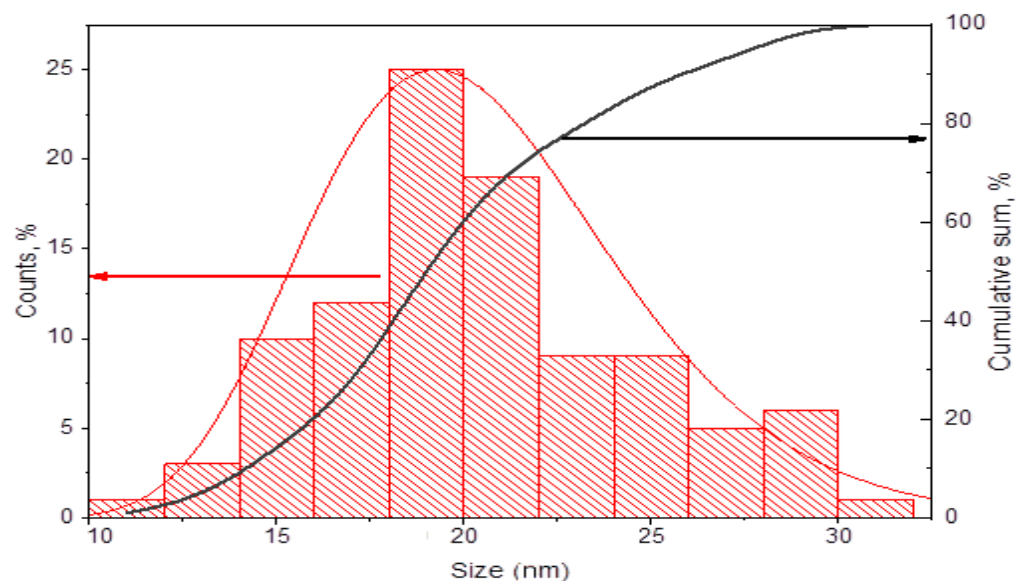
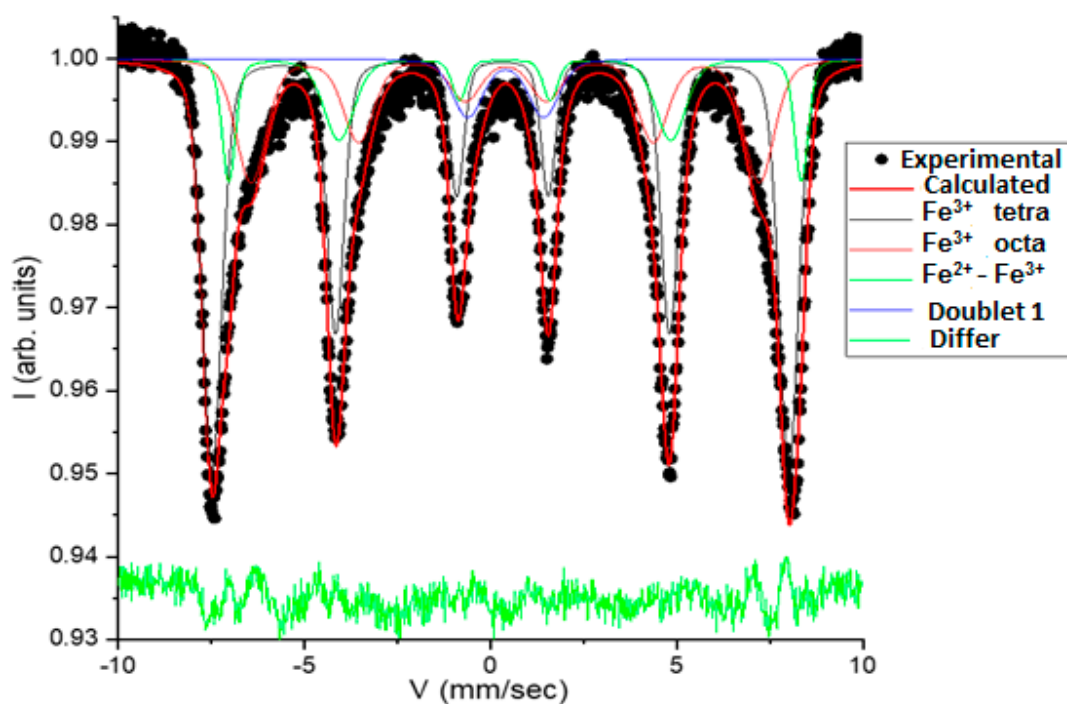


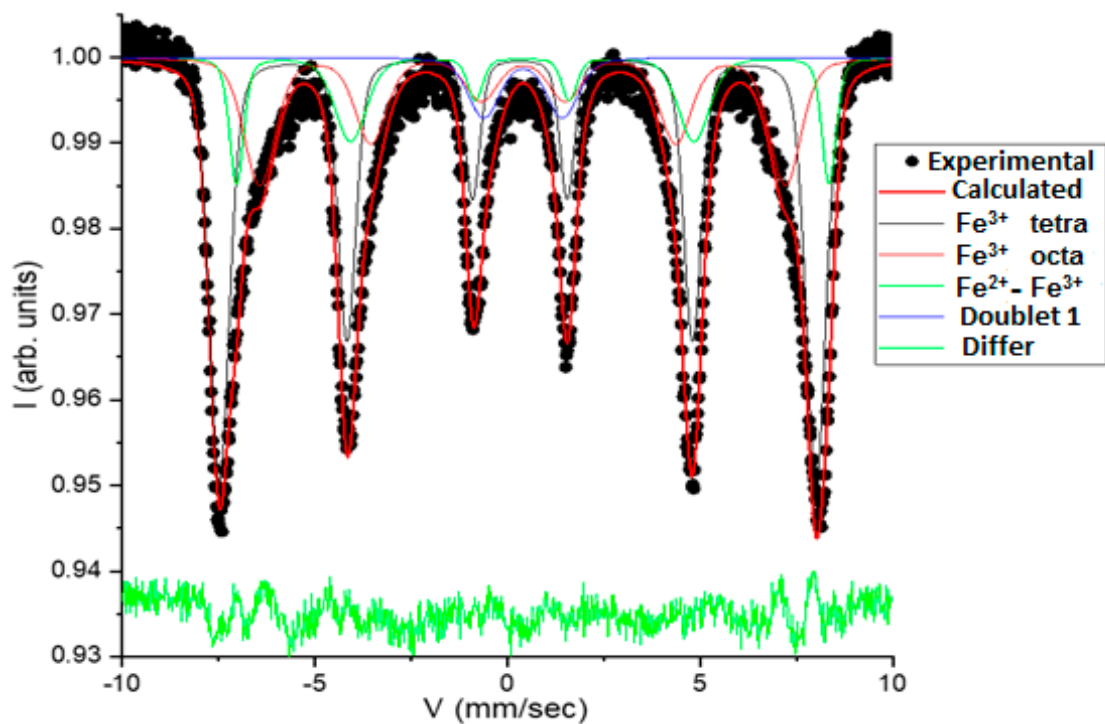
Figure 2. Size distribution of magnetite nanoparticles. The black line with an arrow represents the cumulative percentage curve. The red line with a red arrow is the distribution of particles along the largest chord.

Using Mössbauer spectroscopy, we studied the structure and phase composition of composite catalysts. The results of Mössbauer spectroscopy confirmed the structure of Fe_3O_4 . Figure 3 shows the Mössbauer spectrum of Fe_3O_4 , $\text{Fe}_3\text{O}_4/\text{SiO}_2$, and $\text{Fe}_3\text{O}_4/\text{Al}_2\text{O}_3$.

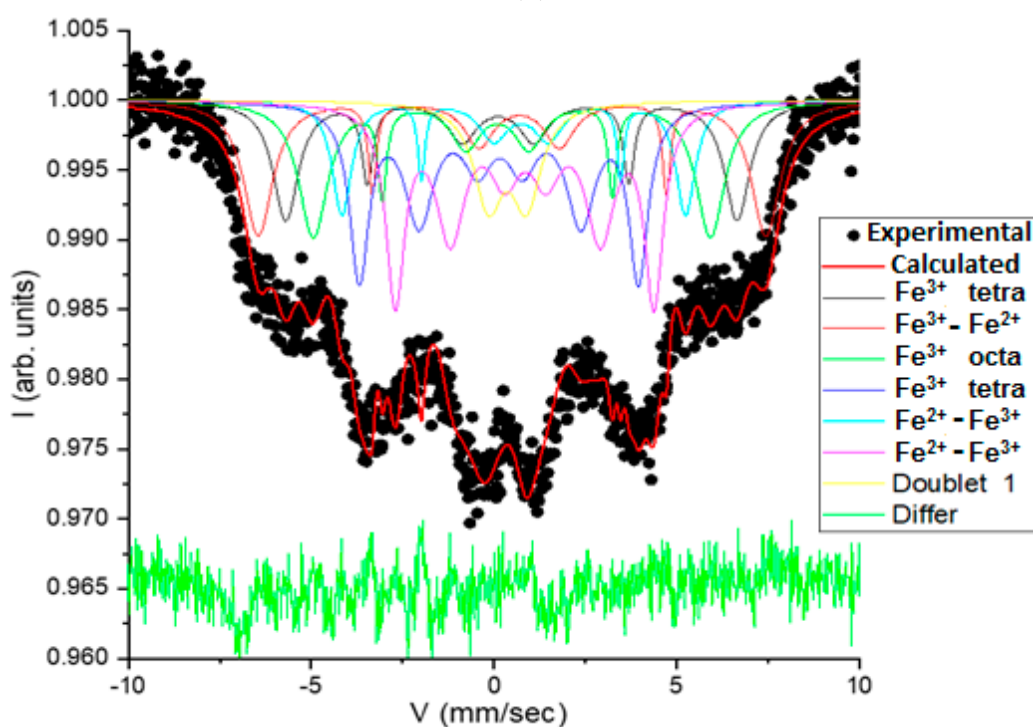


(a)

Figure 3. Cont.



(b)



(c)

Figure 3. Mössbauer spectrum of magnetite Fe_3O_4 (a), Fe_3O_4 stabilized by Al_2O_3 (b) and SiO_2 (c).

As can be seen from Figure 3a, the Mössbauer spectrum of magnetite nanoparticles at room temperature can be considered as consisting of a doublet and three sextets with similar parameters, corresponding to trivalent iron ions in the A and B sublattices; in the B sublattice, iron cations are in two powers oxidation of Fe^{2+} , Fe^{3+} . The parameters of magnetite sextets and doublets are given in Table 1.

Table 1. Parameters of magnetite sextets and doublets.

No	Name	Is, MM/c	Qs, mm/s	H, keV	S _{relative} , %	G, mm/s
1-C	Fe ³⁺ _tetrahedron	0.2898	−0.0545	480.95	51.29	0.6221
2-C	Fe ³⁺ _octahedron	0.3966	−0.0200	423.85	25.99	0.9699
3-C	Fe ²⁺ _Fe ³⁺ _octahedron	0.5192	0.2737	477.61	16.57	0.9699
4-D	Doublet_1	0.4062	2.0478	-	6.15	0.9700

Note: Is is isomer shift, mm/s; Qs is quadrupole splitting, mm/s; H is the magnetic field on Fe nuclei, mm/s; S is the area of the component; G is the line width, mm/s.

These sextets are characterized by the following parameters: Is/ α -Fe = 0.2898 mm/s and N_{effective} = 480.95 keV are typical for Fe³⁺ ions in a tetrahedral environment, while sextets with higher values of the isomer shift Is/ α -Fe = 0.5192 mm/s and N_{effective} = 477.61 keV refer to ⁵⁷Fe nuclei in octahedral positions.

The intermediate value between the isomeric shifts for Fe²⁺ and Fe³⁺ is explained by the presence of Fe²⁺ and Fe³⁺ ions in the octahedral positions and the 3-valent iron ion in the tetrahedral positions, which corresponds to the structural formula of pure magnetite Fe₃O₄, which is spinel. Quadrupole doublet D₁ –can correspond to Fe³⁺ atoms in the structure of small magnetite particles.

The parameters of sextets and doublets of the obtained composite catalysts Fe₃O₄/SiO₂, Fe₃O₄/Al₂O₃ are given in Tables 2 and 3.

Table 2. Parameters of sextets and doublets of Fe₃O₄/SiO₂.

No	Name	Is, MM/c	Qs, mm/s	H, keV	S _{relative} , %	G, mm/s
1-C	Fe ³⁺ - tetrahedron	0.2870	0.2215	400.32	17.20	0.9699
2-C	Fe ³⁺ _Fe ²⁺ _ octahedron	0.6700	−0.2000	444.31	12.14	0.9700
3-C	Fe ³⁺ _ octahedron	0.3127	0.3193	351.52	15.64	0.9698
4-C	Fe ³⁺ _ tetrahedron	0.1500	0.0481	245.82	18.08	0.6017
5-C	Fe ²⁺ _Fe ³⁺ _ octahedron	0.6053	−0.1704	303.71	12.79	0.7540
6-C	Fe ²⁺ -Fe ³⁺ _ octahedron	0.8727	0.0017	228.28	19.40	0.5934
7-D	Doublet_1	0.3690	1.0407		4.76	0.9699

Table 3. Parameters of sextets and doublets of Fe₃O₄/Al₂O₃.

No	Name	Is, MM/c	Qs, mm/s	H, keV	S _{relative} , %	G, mm/s
1-C	Fe ³⁺ _ tetrahedron	0.2966	0.3630	383.50	12.17	0.8444
2-C	Fe ³⁺ _Fe ²⁺ _ octahedron	0.5962	−0.2000	431.43	14.16	0.9700
3-C	Fe ³⁺ _ octahedron	0.2926	0.3958	337.47	14.52	0.9698
4-C	Fe ³⁺ _ tetrahedron	0.1500	−0.0295	237.17	20.37	0.6390
5-C	Fe ²⁺ _Fe ³⁺ _ octahedron	0.6405	−0.2000	291.97	9.26	0.6401
6-C	Fe ²⁺ _Fe ³⁺ _ octahedron	0.8502	−0.0190	219.76	22.56	0.6205
7-D	Doublet_1	0.3690	1.0407	-	6.95	0.9699

The Mössbauer spectra of the obtained composite catalysts Fe₃O₄/SiO₂, Fe₃O₄/Al₂O₃ showed the presence of ferric ions in the tetrahedral environment and the presence of Fe²⁺ and Fe³⁺ in the octahedral environment, and there is also a doublet spectrum. The parameters of this doublet included isomeric shift Is and quadrupole splitting. These characteristics are associated with the appearance of a phase: quartz SiO₂ or α -Al₂O₃.

According to the results of X-ray diffraction analysis, in addition to the crystalline phase of magnetite, there are phases of SiO_2 , quartz and $\alpha\text{-Al}_2\text{O}_3$, which are associated with a shift of isomers and an average magnetic hyperfine field. Additionally, the decrease in effective fields can be explained by a decrease in the size of magnetite particles stabilized by silicon and aluminum oxides (the particle diameter is less than ~ 10 nm). Surface stabilization leads to a decrease in the size of magnetite nanocrystals in nanocomposites.

The results of SEM and the energy-dispersive analysis spectra are demonstrated in Figure 4 ($\text{Fe}_3\text{O}_4/\text{Al}_2\text{O}_3$) and Figure 5 ($\text{Fe}_3\text{O}_4/\text{SiO}_2$).

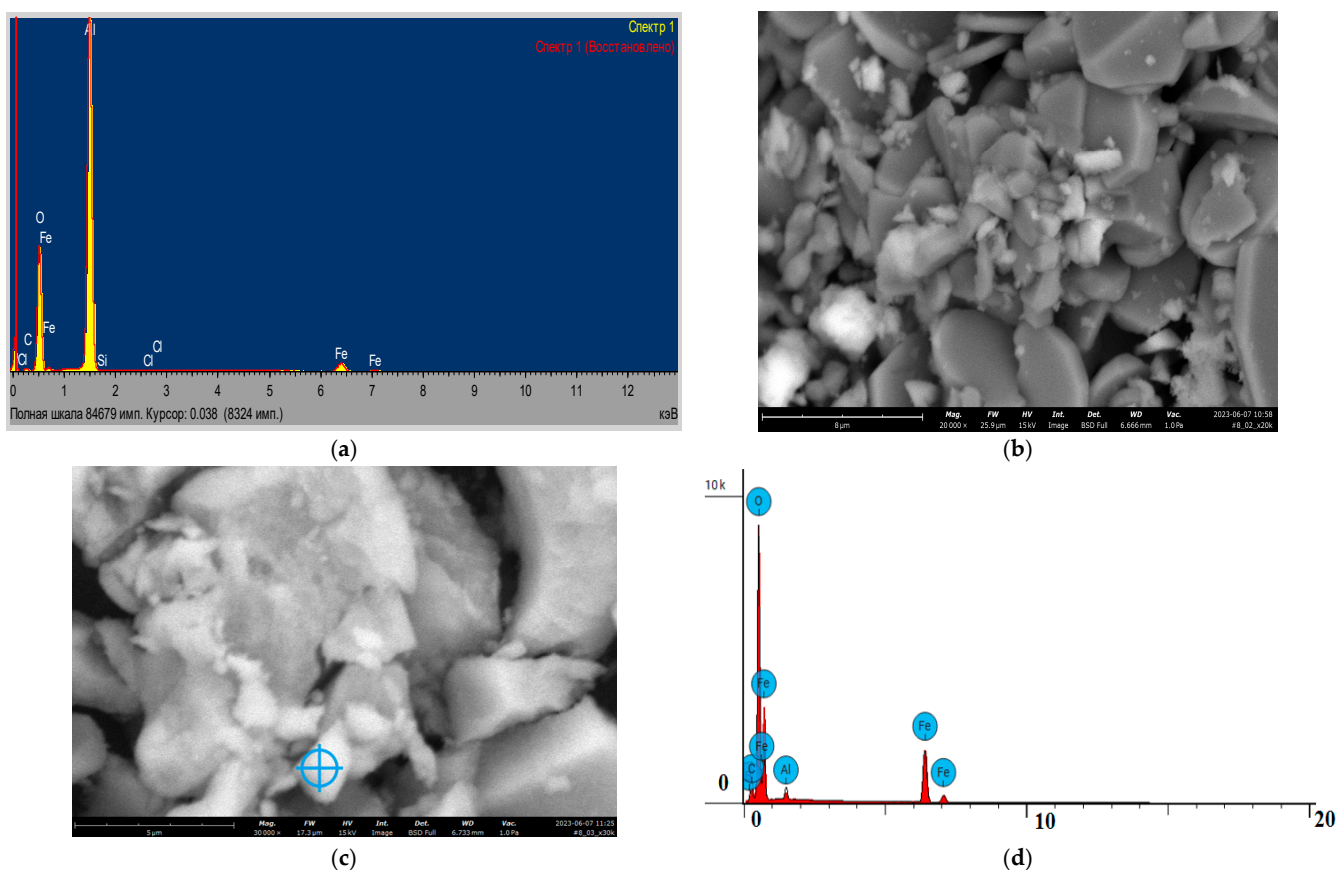


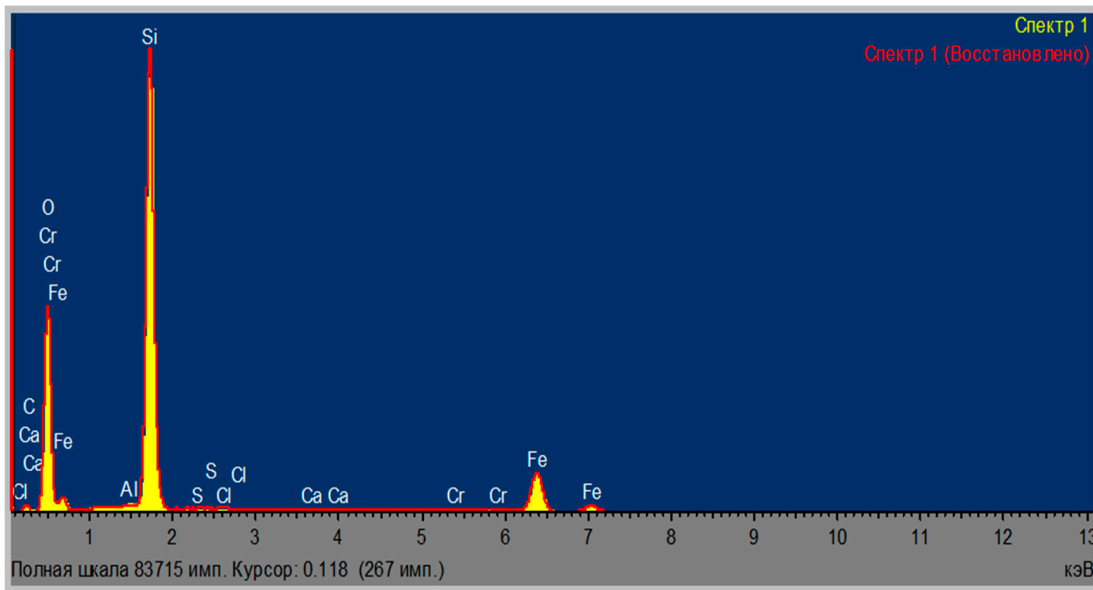
Figure 4. $\text{Fe}_3\text{O}_4/\text{Al}_2\text{O}_3$: (a) and (d) X-ray fluorescence spectrum; (b) and (c) SEM images (the image magnification is 20,000).

The content of elements for a $\text{Fe}_3\text{O}_4/\text{Al}_2\text{O}_3$ (atomic concentration/weight concentration, %) in the synthesized $\text{Fe}_3\text{O}_4/\text{Al}_2\text{O}_3$ based on the elemental analysis (Figure 4d) is as follows: oxygen, 66.616/37.463; aluminum, 2.951/2.797; iron, 30.433/59.740.

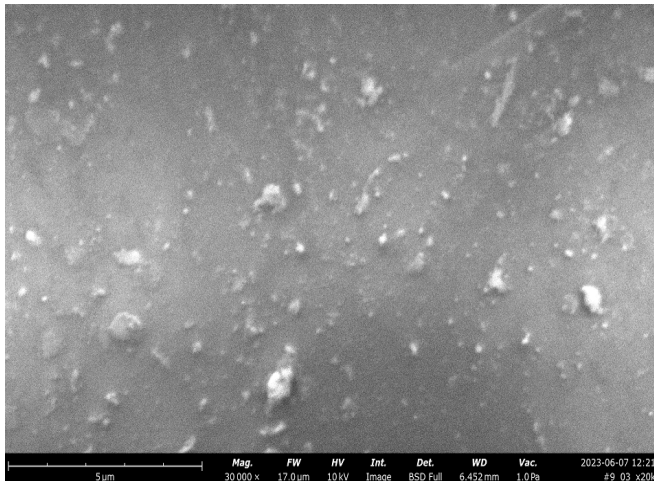
The content of elements (%) for a $\text{Fe}_3\text{O}_4/\text{SiO}_2$ in the synthesized catalyst based on the elemental analysis (Figure 5a) is as follows: O (45.70); Al (0.12); Si (38.25); S (0.05); Cl (0.04); Ca (0.04); Cr (0.15); Fe (15.65).

To evaluate the surface of magnetite, the IR–Fourier spectroscopy method was used (Figure 6). Magnetite has absorption bands $620\text{--}650\text{ cm}^{-1}$, which characterize the vibrations of the Fe–O bonds of magnetite, the absorption bands in the region of 892, 976, and 1108 cm^{-1} belong to the deformation vibrations of the Fe–OH groups [62]. Absorption bands in the range of $2900\text{--}3200\text{ cm}^{-1}$ correspond to vibrations of hydroxyl groups on the surface of magnetite and water and indicate the presence of hydrogen bonds [63,64]. The absorption bands in the region of 1636 cm^{-1} are caused by deformation vibrations of water molecules adsorbed on the surface of magnetite. After stabilization of the surface of magnetite with SiO_2 and Al_2O_3 , changes occur in the spectra of magnetic nanocomposites. Thus, upon stabilization of magnetite SiO_2 , a decrease in the intensity of absorption bands

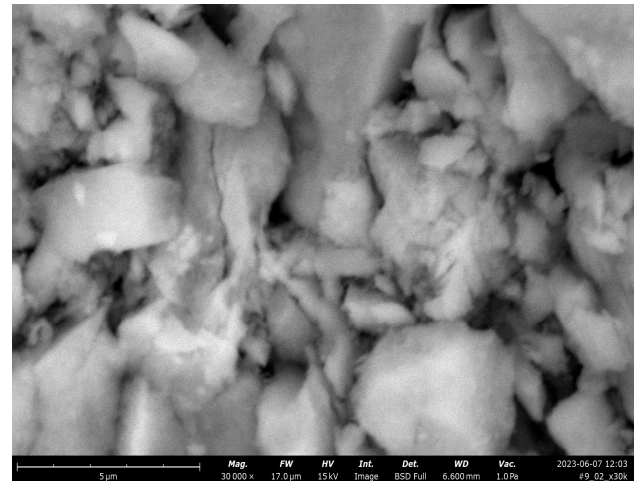
in the region of 1108 cm^{-1} , corresponding to deformation vibrations of Fe–OH, is observed. The absorption bands at 892 cm^{-1} and 976 cm^{-1} associated with the disappearance of Fe–OH vibrations. According to literature data [65,66], absorption bands in the range of $800\text{--}960\text{ cm}^{-1}$ and $1052\text{--}1108\text{ cm}^{-1}$ are typical for Si–O and Si–O–Si bonds. Absorption bands appear in the $\text{Fe}_3\text{O}_4/\text{SiO}_2$ IR spectrum at $864, 808, 1056,$ and 1086 cm^{-1} are associated with silicon oxide oscillations. It is possible to assume the probability of the formation of bonds on the surface of magnetite and the presence of the SiO_2 phase. This is confirmed by the results of the X-ray diffraction analysis.



(a)



(b)



(c)

Figure 5. $\text{Fe}_3\text{O}_4/\text{SiO}_2$: (a) X-ray fluorescence spectrum; (b) and (c) -SEM images (the image magnification is 30,000).

It is known that the IR spectra of Al_2O_3 are characterized by the presence of absorption bands in the region of stretching vibrations of OH groups (νOH) at $3170\text{--}3600\text{ cm}^{-1}$, and the presence of an absorption band at 1637 cm^{-1} indicates a bending vibration of OH groups [67,68]. Examination of the IR spectra of Al_2O_3 -stabilized magnetic composites shows that the absorption bands at 892 cm^{-1} and 976 cm^{-1} associated with Fe–OH vibrations disappear, the presence of an absorption band from 1036 cm^{-1} and 1201 cm^{-1} is observed, as well as an absorption band at 1321 cm^{-1} and 1654 cm^{-1} on the surface of nanocomposites, which are characteristic of Al–O–bonds.

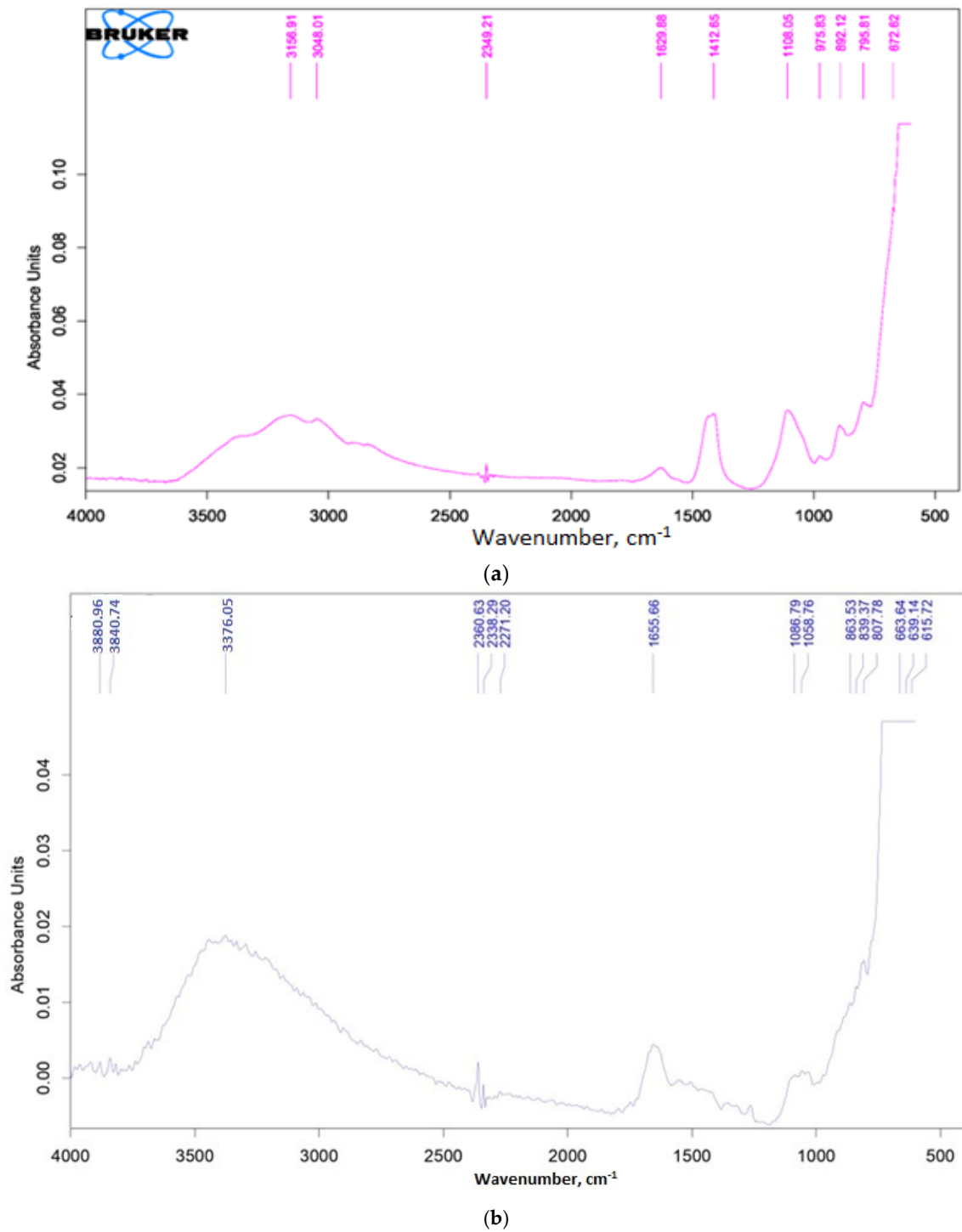


Figure 6. Cont.

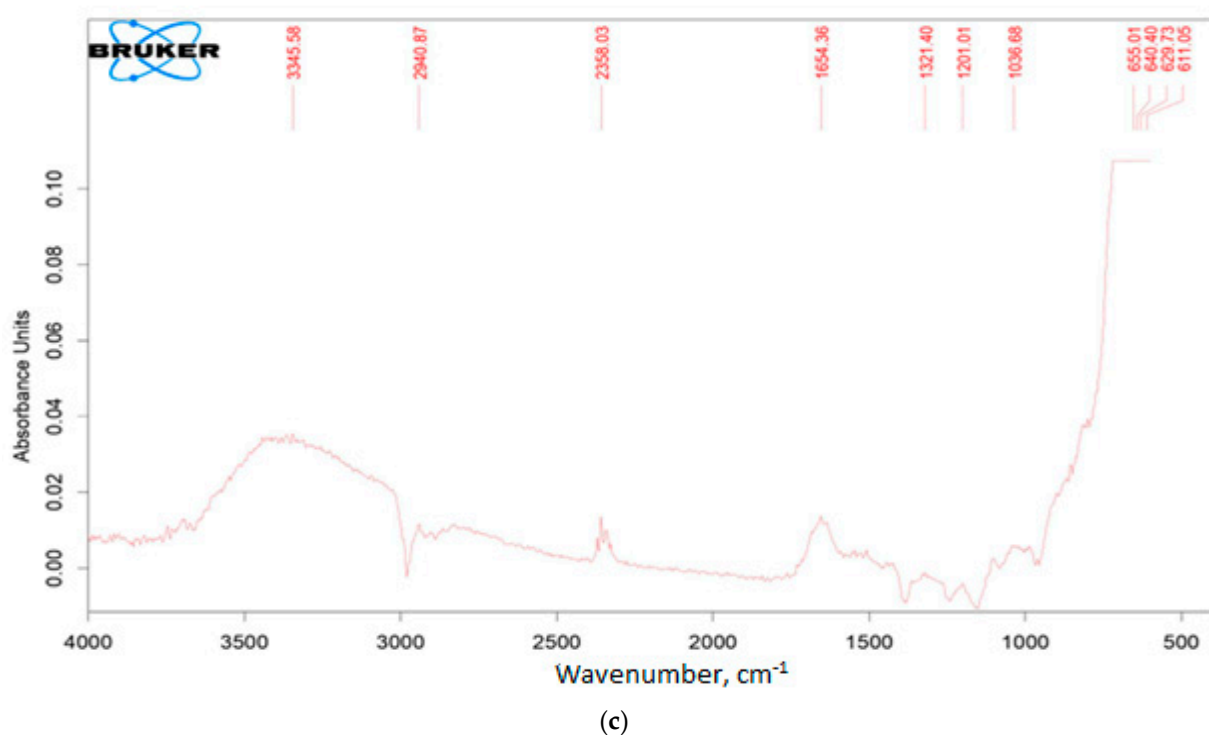


Figure 6. IR spectra: (a) pure magnetite; (b) magnetite stabilized with SiO₂; (c) magnetite stabilized with Al₂O₃.

3.2. Catalysts Testing in the Oxidation Reaction

In the presence of the obtained composite catalysts (Fe₃O₄, Fe₃O₄/SiO₂, Fe₃O₄/Al₂O₃), the oxidation of phenol was investigated under the optimal conditions studied in the course of the research. Figure 7 shows typical conversion curves for the oxidation of phenol with oxygen. The most efficient oxidation of phenol occurs on Fe₃O₄/SiO₂.

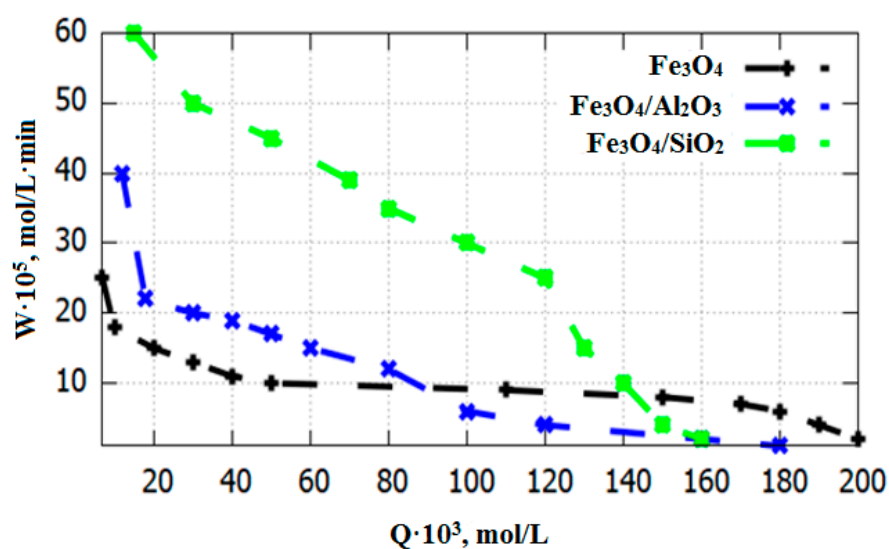


Figure 7. Oxidation of phenol with oxygen on the catalysts: Fe₃O₄, Fe₃O₄/Al₂O₃, and Fe₃O₄/SiO₂: dependence of oxygen absorption rate from the amount of oxygen absorbed, at T = 343 K, P_{atm} = 93.7 kPa, pH = 5–6.

The initial rate of phenol oxidation on Fe₃O₄ stabilized on SiO₂ is more than two times higher than on Fe₃O₄.

The UV spectra of the solutions during the oxidation of phenol with a given concentration were studied. Results were noted for a decrease in optical density D at the phenol absorption wavelength of 270 nm over time. On the UV spectrum of the initial solution in the wavelength range of 190–320 nm, there is an absorption band of phenol at 271.5 nm (Figure 8). A decrease in optical density D at a given wavelength, the appearance of an absorption band at a wavelength of 240–245 nm and a weak band at 430 nm, characteristic of benzoquinone, were revealed. It can be assumed that the phenol content in the solution decreases as its oxidation to benzoquinone increases. This circumstance confirms the data of the IR spectrum of the product.

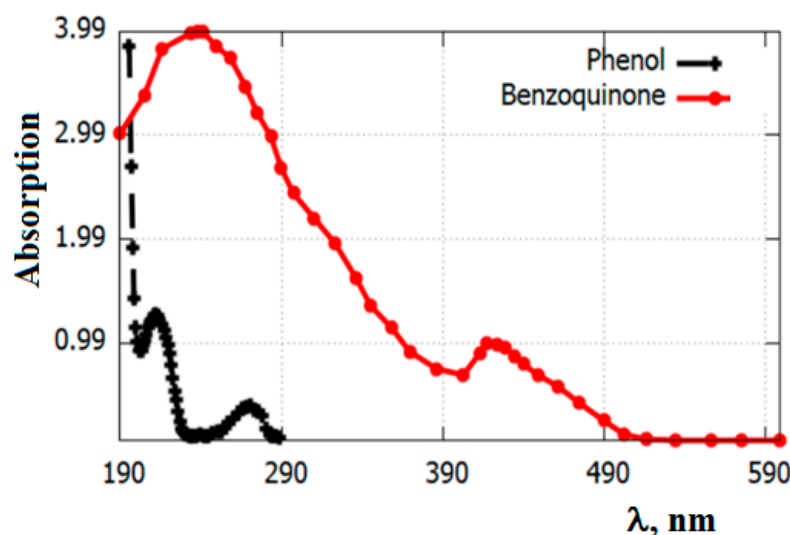


Figure 8. Absorption spectra of the initial aqueous solution of phenol and the reaction product.

In the IR spectrum of the product, absorption bands in the region of 1644 cm^{-1} are characteristic of the vibrations of the C=O bonds of the carbonyl group of benzoquinone, and the detected peaks at 1353 cm^{-1} and 1229 cm^{-1} can be related to the vibrations of the C–H and C–C bonds of the quinone ring [65–70]. As can be seen from Figure 8, the optical density of the reaction product is reduced compared to the initial solution.

Thus, based on the data of UV and IR spectroscopy, magnetic composites based on iron oxide show their efficiency in the oxidation of phenol with oxygen.

Additionally, in the presence of $\text{Fe}_3\text{O}_4/\text{SiO}_2$, the oxidation of pyrocatechol and cresol with oxygen was studied under optimal conditions. It is known from the literature that polyhydric phenols (hydroquinone and pyrocatechol), like phenol, are weak acids with several dissociation constants. They are characterized by a reaction with FeCl_3 , leading to the formation of colored products: pyrocatechol gives a green color, hydroquinone gives a black-violet color. Like phenol, polyhydric phenols easily undergo electrophilic substitution reactions. They are easily oxidized in air; the oxidation of pyrocatechol and hydroquinone occurs especially easily with the formation of 1,2-benzoquinone and 1,4-benzoquinone, respectively.

Figure 9 shows the conversion curves of the oxidation of phenol derivatives with oxygen. From the experimental results presented in Figure 8, it is clear that catechol oxidizes at the highest rate.

To determine the reaction order with respect to the substrate, the effect of phenol concentration on the rate of its oxidation of $\text{Fe}_3\text{O}_4/\text{SiO}_2$ was studied. Figure 10 presents experimental results demonstrating the effect of the initial concentration of phenol on the rate of its oxidation by oxygen in the presence of $\text{Fe}_3\text{O}_4/\text{SiO}_2$ at 333 K. With an increase in the concentration of phenol in the range from 0.5×10^{-1} to 3.0×10^{-1} mol/L the oxidation

rate increases, and the amount of absorbed oxygen increases proportionally in accordance with the stoichiometry of reaction (1):

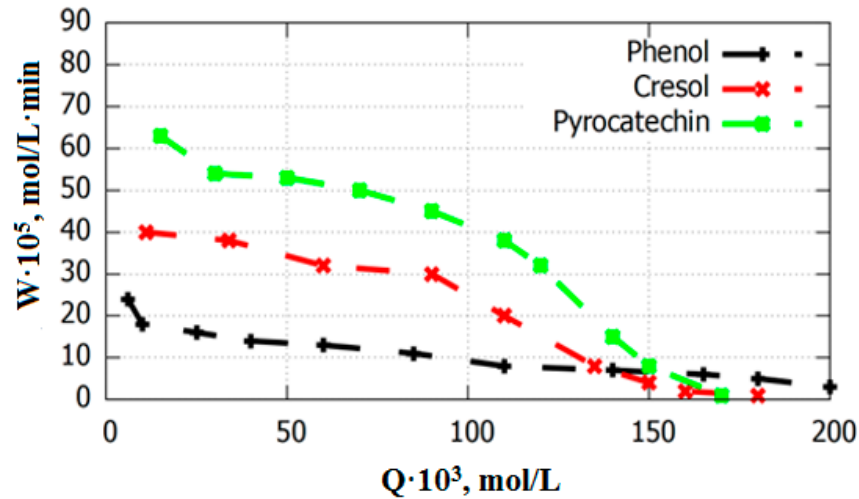
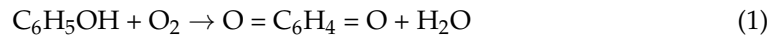


Figure 9. Oxidation of phenol, pyrocatechol and cresol with oxygen in the presence of $\text{Fe}_3\text{O}/\text{SiO}_2$: dependence of the rate of oxygen absorption on the amount of absorbed oxygen at $T = 343 \text{ K}$, $P_{\text{atm}} = 93.7 \text{ kPa}$, $\text{pH} = 5\text{--}6$.

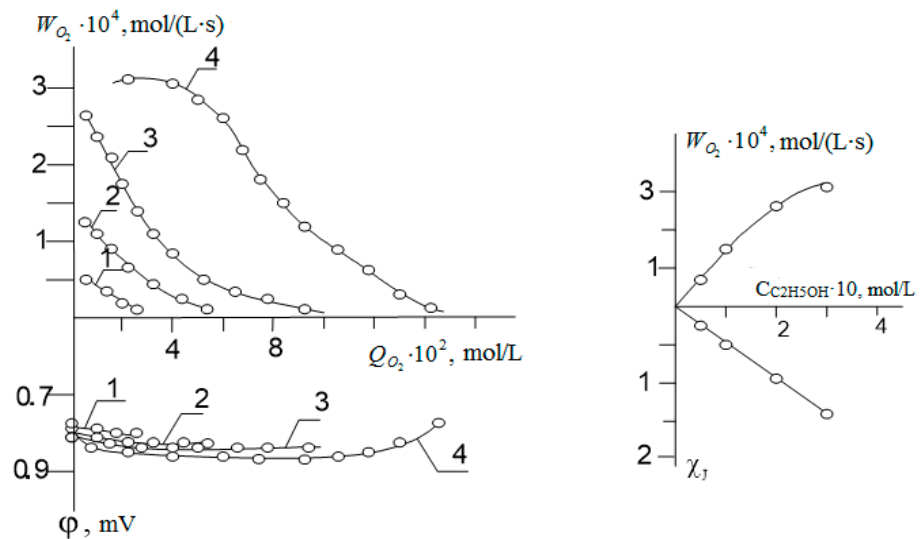


Figure 10. Oxidation of phenol with oxygen in the presence of $\text{Fe}_3\text{O}_4/\text{SiO}_2$ at $T = 333 \text{ K}$, $\text{C}_{\text{C}_2\text{H}_5\text{OH}} \cdot 10, \text{ mol/L}$: 1–0.5; 2–1.0; 3–2.0; 4–3.0.

There is a linear relationship between the amount of absorbed oxygen and the initial concentration of phenol in the solution; the $Q_{\text{O}_2}/\text{C}_{\text{C}_6\text{H}_5\text{OH}}$ ratio is equal to unity. From the nature of the conversion curves of phenol oxidation on $\text{Fe}_3\text{O}_4/\text{SiO}_2$ at constant pressure and temperature, it is clear that the process of phenol oxidation occurs at the maximum rate during the first 10 min, and then the reaction rate gradually decreases. The order of the reaction by substance, which is determined by the tangent of the angle from the logarithmic dependence of the initial reaction rate on the concentration of the substance, on the studied $\text{Fe}_3\text{O}_4/\text{SiO}_2$ catalyst is close to 1. The calculated reaction rate constant, according to the first-order equation, is constant until the absorption of 30–50% of the calculated amount of oxygen.

In the IR spectra of the product (Figure 11, red lines), spectral bands appear in the region of 1630–1644 cm^{-1} , which is characteristic of p-benzoquinone. The dependence of the rate of phenol oxidation on the initial concentration of phenol in solution is described by a first-order equation: $W_{\text{O}_2} = k_1 \times C_{\text{C}_6\text{H}_5\text{OH}}$, at 313 K, $k_1 = 0.68 \text{ min}^{-1}$.

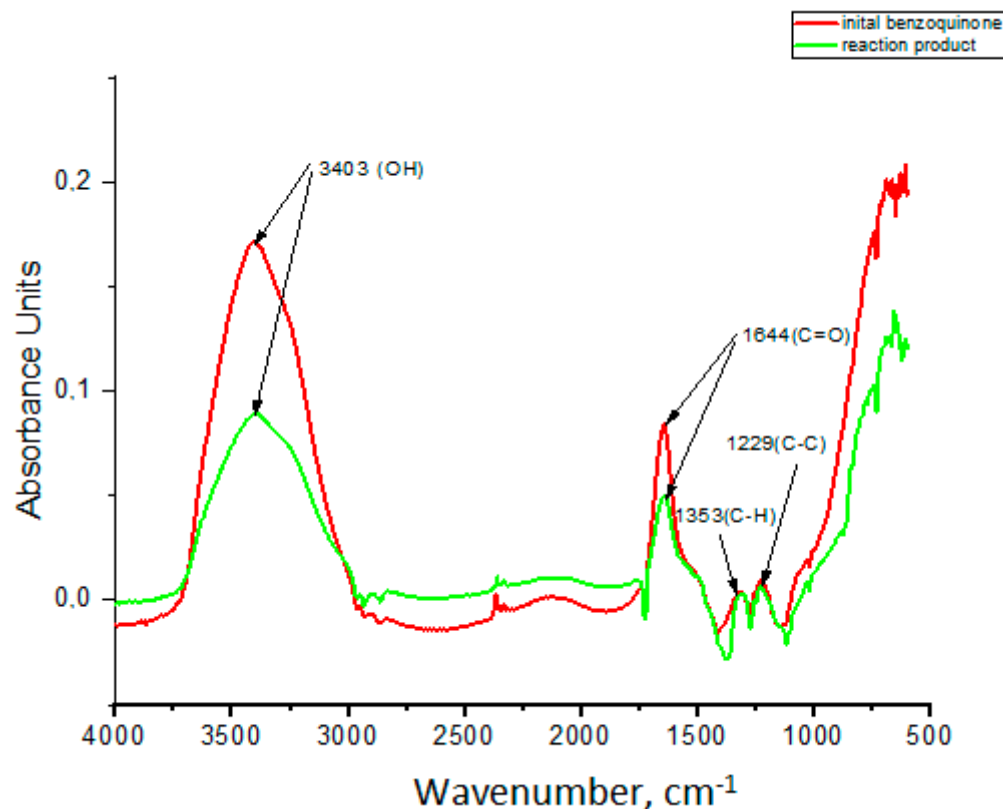


Figure 11. The IR spectra of the product of oxidation of phenol with oxygen in the presence of $\text{Fe}_3\text{O}_4/\text{SiO}_2$ at $T = 333 \text{ K}$.

The effect of temperature (303–333 K) on the rate of phenol oxidation was studied at a constant oxygen pressure of 1.0 MPa. At temperatures of 303–313 K, incomplete absorption of the calculated amount of oxygen is observed; analysis data indicate non-selective oxidation of phenol. Intermediate products were discovered—catechin, hydroquinone, formic acid) oxidation products. In the temperature range of 303–333 K on the catalyst under study, the obtained dependences are described by second-order reaction equations. The apparent activation energy, calculated from the Arrhenius equation and from the dependence of $\log k$ on $1/T$, in the temperature range under study is 51.2 kJ/mol. The chemical inertness of the oxygen molecule is due to the high binding energy and spin prohibition in chemical reactions of molecular oxygen. The oxidizing agent can only be activated oxygen in the form of the superoxide anion $\text{O}_2^{\bullet -}$ or the HO^\bullet radical formed from it with the sequential reduction of the O_2 molecule with one, two or three electrons, respectively.

Thus, nanocomposite catalysts (Fe_3O_4 , $\text{Fe}_3\text{O}_4/\text{SiO}_2$, $\text{Fe}_3\text{O}_4/\text{Al}_2\text{O}_3$) have been synthesized. It can be concluded that the introduction of SiO_2 and Al_2O_3 in optimal concentrations leads to the creation of a protective adsorption layer that ensures aggregative and sedimentation stability of the dispersion of magnetic particles. The resulting composite catalysts $\text{Fe}_3\text{O}_4/\text{SiO}_2$ and $\text{Fe}_3\text{O}_4/\text{Al}_2\text{O}_3$ are significantly more effective than particles of unmodified magnetite. The catalytic properties of composite catalysts correlate with their specific surface area introduced during synthesis. The developed composite catalysts were tested in the process of the oxidation of phenol and phenol-containing compounds in aqueous solutions. UV and IR spectroscopy data confirm that stabilized composite catalysts are active and effective in the oxidation of phenol and phenol-containing compounds with oxygen.

4. Conclusions

Magnetite-based nanomaterials are widely used as part of composite systems in medicine, biotechnology and engineering, and catalysts based on nanosized magnetite have high chemical activity. This work discusses the synthesis of magnetite nanoparticles and composite catalysts based on magnetite stabilized by silicon and aluminum oxides. The properties of composite catalysts (Fe_3O_4 , $\text{Fe}_3\text{O}_4/\text{SiO}_2$, and $\text{Fe}_3\text{O}_4/\text{Al}_2\text{O}_3$) for the catalytic oxidation of phenol and its derivatives have been synthesized and studied. The results of X-ray diffraction analysis of the resulting magnetite demonstrated the presence of a spinel phase with space group $\text{Fd}\bar{3}\text{m}$ and lattice parameter $a = 0.8386$ nm. The only crystalline phase present in the sample is magnetite, which is responsible for the higher magnetic properties. The results of Mössbauer spectroscopy confirmed the structure of Fe_3O_4 . The average size of magnetite crystallites, calculated using the Debye–Scherrer formula, is 16–20 nm. Using the methods of IR-Fourier spectroscopy and X-ray diffraction analysis, SiO_2 and Al_2O_3 phases were identified on the surface of magnetite in magnetic composites. When magnetite is stabilized with aluminum and silicon oxides, the average size of nanoparticles decreases to 9–10 nm. Based on a study of the formation of Fe_3O_4 nanoparticles and composite particles $\text{Fe}_3\text{O}_4/\text{SiO}_2$ and $\text{Fe}_3\text{O}_4/\text{Al}_2\text{O}_3$ and their structural characteristics, it was established that the modification of the magnetite surface with aluminum and silicon oxides leads to a significant increase in their surface and a decrease in the size of magnetite nanocrystallites in nanocomposites compared to unmodified magnetite. UV and IR spectroscopy data confirm that the stabilized magnetic composites are active and efficient in the oxidation of phenol with oxygen. Based on UV and IR spectroscopy data, it was concluded that composite catalysts based on magnetite are effective in the oxidation of phenol, pyrocatechol and cresol with oxygen.

Author Contributions: Conceptualization, B.T.D., L.R.S. and D.M.; methodology, B.T.D. and T.V.S.; software, L.R.S. and A.A.B.; validation, B.T.D., L.R.S. and M.A.K.; formal analysis, B.T.D., L.R.S., A.A.B. and M.A.K.; investigation, D.M., B.T.D., L.R.S., A.A.B. and M.A.K.; resources, D.M. and B.T.D.; data curation, D.M., T.V.S. and B.T.D.; writing—original draft preparation, B.T.D. and L.R.S.; writing—review and editing, B.T.D. and L.R.S.; visualization, T.V.S. and A.A.B.; supervision, D.M. and B.T.D.; project administration, D.M.; funding acquisition, D.M., T.V.S. and B.T.D. All authors have read and agreed to the published version of the manuscript.

Funding: This research was funded by the Science Committee of the Ministry of Education and Science of the Republic of Kazakhstan, grant No. AP09260687 “Technology for the extraction and utilization of toxic compounds of industrial wastewater”.

Data Availability Statement: Data are contained within the article.

Conflicts of Interest: The authors declare no conflicts of interest.

References

1. Bierkens, M.F.P. Global hydrology 2015: State, trends, and directions. *Water Resour. Res.* **2015**, *51*, 4923–4947. [[CrossRef](#)]
2. Pedro-Monzonis, M.; Solera, A.; Ferrer, J.; Estrela, T.; Paredes-Arquiola, J. A review of water scarcity and drought indexes in water resources planning and management. *J. Hydrol.* **2015**, *527*, 482–493. [[CrossRef](#)]
3. Carr, G.; Blöschl, G.; Loucks, D.P. Evaluating participation in water resource management: A review. *Water Resour. Res.* **2012**, *48*, W11401. [[CrossRef](#)]
4. Mousazadeh, M.; Khademi, N.; Kabdaşlı, I.; Rezaei, S.; Hajalifard, Z.; Moosakhani, Z.; Hashim, K. Domestic greywater treatment using electrocoagulation-electrooxidation process: Optimisation and experimental approaches. *Sci. Rep.* **2023**, *13*, 15852. [[CrossRef](#)]
5. Haryanto, A.A.B.; Ramelan, A.H.; Budiastuti, M.T.S. Comprehensive study of chromium heavy metal adsorption from textile wastewater using natural composite adsorbent. *Rasayan J. Chem.* **2022**, *15*, 2527–2533. [[CrossRef](#)]
6. Kouacou, K.F.J.; Ouattara, A.; Assémian, A.S.; Yao, K.B. Life cycle assessment of wastewater treatment in a refinery with focus on the desalting process. *Asian J. Water Environ. Pollut.* **2023**, *20*, 1–8. [[CrossRef](#)]
7. Khatri, N.; Tyagi, S. Influences of natural and anthropogenic factors on surface and groundwater quality in rural and urban areas. *Front. Life Sci.* **2015**, *8*, 23–39. [[CrossRef](#)]

8. Dossumova, B.T.; Sassykova, L.R.; Shakiyeva, T.V.; Mukhtaly, D.; Baizhomartov, B.; Kanapiyeva, F.M.; Hideki Kurokawa, H. Natural waters and industrial wastewater, wastewater with phenol-containing compounds, methods of water purification. *Rasayan J. Chem.* **2023**, *16*, 1591–1598. [[CrossRef](#)]
9. Cosgrove, W.J.; Loucks, D.P. Water management: Current and future challenges and research directions. *Water Resour. Res.* **2015**, *51*, 4823–4839. [[CrossRef](#)]
10. Ejraei, A.; Aroon, M.A.; Saravani, A.Z. Wastewater treatment using a hybrid system combining adsorption, photocatalytic degradation and membrane filtration processes. *J. Water Process. Eng.* **2019**, *28*, 45–53. [[CrossRef](#)]
11. Taghipour, S.; Hosseini, S.M.; Ataie-Ashtiani, B. Engineering nanomaterials for water and wastewater treatment: Review of classifications, properties and applications. *New J. Chem.* **2019**, *43*, 7902–7927. [[CrossRef](#)]
12. Crini, G.; Lichtfouse, E. Advantages and disadvantages of techniques used for wastewater treatment. *Environ. Chem. Lett.* **2019**, *17*, 145–155. [[CrossRef](#)]
13. Sharma, P.; Gaur, V.K.; Gupta, S.; Varjani, S.; Pandey, A.; Gnansounou, E.; You, S.; Ngo, H.H.; Wong, J.W.C. Trends in mitigation of industrial waste: Global health hazards, environmental implications and waste derived economy for environmental sustainability. *Sci. Total. Environ.* **2022**, *811*, 152357. [[CrossRef](#)] [[PubMed](#)]
14. Zhang, Z.; Malik, M.Z.; Khan, A.; Ali, N.; Malik, S.; Bilal, M. Environmental impacts of hazardous waste, and management strategies to reconcile circular economy and eco-sustainability. *Sci. Total. Environ.* **2022**, *807*, 150856. [[CrossRef](#)]
15. Henze, M. *Wastewater Treatment: Biological and Chemical Processes*, 3rd ed.; Springer: Berlin, Germany, 2002; pp. 87–112.
16. Sonune, A.; Ghate, R. Developments in wastewater treatment methods. *Desalination* **2004**, *167*, 55–63. [[CrossRef](#)]
17. Whitesides, G. 2030. Technology That Will Change the World. By Rutger van Santen, Djan Khoe und Bram Vermeer. *Angew. Chem. Int. Ed.* **2012**, *124*, 879–880. [[CrossRef](#)]
18. Busca, G.; Berardinelli, S.; Resini, C.; Arrighi, L. Technologies for the removal of phenol from fluid streams: A short review of recent developments. *J. Hazard. Mater.* **2008**, *160*, 265–288. [[CrossRef](#)]
19. Liotta, L.F.; Gruttadauria, M.; Carlo, G.D.; Perrini, G.; Librando, V. Heterogeneous catalytic degradation of phenolic substrates: Catalysts activity. *J. Hazard. Mater.* **2009**, *162*, 588–606. [[CrossRef](#)]
20. Tashmukhambetova, Z.K.; Sassykova, L.R.; Aubakirov, Y.A.; Dangaliyeva, A.K.; Kanatbayeva, M.A.; Rustem, A.E. New catalysts for toluene oxidation technology in the liquid phase. *Mater. Today Proc.* **2020**, *31*, 529–531. [[CrossRef](#)]
21. Tian, X.; Zhang, H.; Hu, C.; Yan, Y. Preparation of microfiber composite nitrogen doped carbon nanotube membranes and their degradation properties of phenol in the structured fixed bed. *J. Environ. Chem. Eng.* **2023**, *11*, 109255. [[CrossRef](#)]
22. Tomita, K.; Oshima, Y. Stability of manganese oxide in catalytic supercritical water oxidation of phenol. *Ind. Eng. Chem. Res.* **2004**, *43*, 7740–7743. [[CrossRef](#)]
23. Droste, R.L.; Gehr, R.L. *Theory and Practice of Water and Wastewater Treatment*; John Wiley & Sons: Hoboken, NJ, USA, 2018; pp. 218–278.
24. Krajnc, M.; Levec, J. Oxidation of phenol over a transition-metal oxide catalyst in supercritical water. *Ind. Eng. Chem. Res.* **1997**, *36*, 3439–3445. [[CrossRef](#)]
25. Wang, Y.; Wang, S.; Guo, Y.; Xu, D.; Gong, Y.; Tang, X.; Ma, H. Oxidative degradation of lurgi coal-gasification wastewater with Mn₂O₃, Co₂O₃, and CuO catalysts in supercritical water. *Ind. Eng. Chem. Res.* **2012**, *51*, 16573–16579. [[CrossRef](#)]
26. Nihemaiti, M.; Miklos, D.B.; Hübner, U.; Linden, K.G.; Drewes, J.E.; Croué, J.P. Removal of trace organic chemicals in wastewater effluent by UV/H₂O₂ and UV/PDS. *Water Res.* **2018**, *145*, 487–497. [[CrossRef](#)] [[PubMed](#)]
27. Silva, C.L.; Garlapalli, R.K.; Tremblay, J.P. Removal of phenol from oil/gas produced water using supercritical water treatment with TiO₂ supported MnO₂ catalyst. *J. Environ. Chem. Eng.* **2017**, *5*, 488–493. [[CrossRef](#)]
28. Baloyi, J.; Ntho, T.; Moma, J. Synthesis and application of pillared clay heterogeneous catalysts for wastewater treatment: A review. *RSC Adv.* **2018**, *8*, 5197–5211. [[CrossRef](#)] [[PubMed](#)]
29. Calleja, G.; Melero, J.A.; Martínez, F.; Molina, R. Activity and resistance of iron-containing amorphous, zeolitic and mesostructured materials for wet peroxide oxidation of phenol. *Water Res.* **2005**, *39*, 1741–1750. [[CrossRef](#)]
30. Maurya, M.R.; Titinchi, S.J.J.; Chand, S. Oxidation of phenol with H₂O₂ catalysed by Cr(III), Fe(III) or Bi(III) N,N'-bis(salicylidene)diethylenetriamine (H₂saldien) complexes encapsulated in zeolite-Y. *J. Mol. Catal. A Chem.* **2003**, *193*, 165–176. [[CrossRef](#)]
31. Barrault, J. Catalytic wet peroxide oxidation over mixed (Al–Fe) pillared clays. *Appl. Catal. B* **2000**, *27*, L225–L230. [[CrossRef](#)]
32. Baabu, P.R.S.; Kumar, H.K.; Gumpu, M.B.; Babu, K.J.; Kulandaisamy, A.J.; Rayappan, J.B.B. Iron Oxide Nanoparticles: A Review on the Province of Its Compounds, Properties and Biological Applications. *Materials* **2023**, *16*, 59. [[CrossRef](#)]
33. Wanna, W.H.; Janmanchi, D.; Thiyagarajan, N.; Ramu, R.; Tsai, Y.F.; Yu, S.S.F. Selective oxidation of simple aromatics catalyzed by nano-biomimetic metal oxide catalysts: A mini review. *Front. Chem.* **2020**, *8*, 589178. [[CrossRef](#)] [[PubMed](#)]
34. Arefieva, O.D.; Vasilyeva, M.S.; Kuryavy, V.G.; Ustinov, A.Y.; Zemnukhova, L.A.; Gushchina, D.D. Oxidative destruction of phenol on Fe/SiO₂ catalysts. *Water Sci. Technol.* **2020**, *81*, 2189–2201. [[CrossRef](#)] [[PubMed](#)]
35. Guélou, E.; Barrault, J.; Fournier, J.; Tatibouët, J.-M. Active iron species in the catalytic wet peroxide oxidation of phenol over pillared clays containing iron. *Appl. Catal. B* **2003**, *44*, 1–8. [[CrossRef](#)]
36. Abid, M.F.; Alwan, G.M.; Abdul-Ridha, L.A. Study on catalytic wet air oxidation process for phenol degradation in synthetic wastewater using trickle bed reactor. *Arab. J. Sci. Eng.* **2016**, *41*, 2659–2670. [[CrossRef](#)]

37. Nimz, M.; Lietz, G.; Völter, J.; Lázár, K.; Guzzi, L. Direct conversion of syngas to aromatics on FePd/SiO₂ catalyst. *Catal. Lett.* **1988**, *1*, 93–98. [[CrossRef](#)]
38. Iorio, E.D.; Colombo, C.; Cheng, Z.; Capitani, G.; Mele, D.; Ventrucci, G.; Angelico, R. Characterization of magnetite nanoparticles synthesized from Fe(II)/nitrate solutions for arsenic removal from water. *J. Environ. Chem. Eng.* **2019**, *7*, 102986. [[CrossRef](#)]
39. Sassykova, L.; Shakiyeva, T.; Dossuymova, B.; Ilmuratova, M.S.; Mukhtaly, D.; Zhaxibayeva, Z.M.; Sassykova, A.; Baizhomartov, B. Catalysts, magnetic composites for removal of phenol-containing compounds from wastewater. *Rasayan J. Chem.* **2023**, *16*, 1605–1612. [[CrossRef](#)]
40. Datsko, T.; Zelentsov, V.; Dvornikov, D. Advanced Nanotechnology-Based Approaches to Waste Water Purification from Organic Pollutants. *IFMBE Proc.* **2024**, *91*, 134–146.
41. Khabibullin, V.R.; Stepanov, G.V. Effect of a low-frequency magnetic field on the release of heat by magnetic nanoparticles of different shapes. *Russ. J. Phys. Chem. A* **2020**, *94*, 439–444. [[CrossRef](#)]
42. Ayati, A.; Ahmadpour, A.; Bamoharram, F.F.; Tanhaei, B.; Mänttari, M.; Sillanpää, M. A review on catalytic applications of Au/TiO₂ nanoparticles in the removal of water pollutant. *Chemosphere* **2014**, *107*, 163–174. [[CrossRef](#)]
43. Jung, H.; Kim, J.W.; Choi, H.; Lee, J.H.; Hur, H.G. Synthesis of nanosized biogenic magnetite and comparison of its catalytic activity in ozonation. *Appl. Catal. B Environ.* **2008**, *83*, 208–213. [[CrossRef](#)]
44. Bai, Y.; Wang, L.; Lu, S.; Zhang, A.; Qu, W.; He, K.; Hu, N. Research on ultrafast catalytic degradation of heterocyclic compounds by the novel high entropy catalyst. *J. Environ. Chem. Eng.* **2023**, *11*, 110703. [[CrossRef](#)]
45. Bukharkina, T.V.; Digurov, N.G.; Mil'K, S.B.; Shelud'Ko, A.B. Development of the Process of p-Nitroacetophenone and Benzoic Acid Manufacture by the Liquid-Phase Oxidation of Aromatic Compounds. *Org. Process. Res. Dev.* **1999**, *3*, 404–408. [[CrossRef](#)]
46. Pestunova, O.P.; Ogorodnikova, O.L.; Parmon, V.N. Studies on the Phenol Wet Peroxide Oxidation in the Presence of Solid Catalysts. *Chem. Sustain. Dev.* **2003**, *11*, 227–232.
47. Timofeeva, M.; Khankhasaeva, S.; Chesalov, Y.; Tsybulya, S.; Panchenko, V.; Dashinamzhilova, E. Synthesis of Fe, Al-pillared clays starting from the Al, Fe-polymeric precursor: Effect of synthesis parameters on textural and catalytic properties. *Appl. Catal. B Environ.* **2009**, *88*, 127–134. [[CrossRef](#)]
48. Brussino, P.; Gross, M.S.; Ulla, M.A.; Banús, E.D. Copper and iron-based monolithic catalysts for phenol Catalytic Wet Peroxide Oxidation (CWPO): Support and iron effects on the catalytic performance. *J. Environ. Chem. Eng.* **2023**, *11*, 110858. [[CrossRef](#)]
49. Catrinescu, C.; Teodosiu, C.; Macoveanu, M.; Miede-Brendlé, J.; Dred, R.L. Catalytic wet peroxide oxidation of phenol over Fe-exchanged pillared beidellite. *Water Res.* **2003**, *37*, 1154–1160. [[CrossRef](#)]
50. Zambrzycki, C.; Shao, R.; Misra, A.; Streb, C.; Herr, U.; Güttel, R. Iron based core-shell structures as versatile materials: Magnetic support and solid catalyst. *Catalysts* **2021**, *11*, 72. [[CrossRef](#)]
51. Sassykova, L.R.; Dossuymova, B.T.; Ilmuratova, M.S.; Shakiyeva, T.V.; Baizhomartov, B.B.; Sassykova, A.R.; Zhaxibayeva, Z.M.; Abildin, T.S. Development of nanostructured catalysts for catalytic oxidative water purification from organic impurities, including phenolic compounds. *Chim. Techno Acta.* **2023**, *10*, 202310309. [[CrossRef](#)]
52. Dossuymova, B.T.; Shakiyeva, T.V.; Mukhtaly, D.; Sassykova, L.R.; Baizhomartov, B.B.; Subramanian, S. Synthesis, Characterization of magnetic composites and testing of their activity in liquid-phase oxidation of phenol with oxygen. *Chem. Eng.* **2022**, *6*, 68. [[CrossRef](#)]
53. Huang, H.; Zhang, H.; Yan, Y. Preparation of novel catalyst-free Fe₃C nanocrystals encapsulated NCNT structured catalyst for continuous catalytic wet peroxide oxidation of phenol. *J. Hazard. Mater.* **2021**, *407*, 124371. [[CrossRef](#)] [[PubMed](#)]
54. Ovejero, G.; Sotelo, J.L.; Martínez, F.; Gordo, L. Novel heterogeneous catalysts in the wet peroxide oxidation of phenol. *Water Sci. Technol.* **2001**, *44*, 153–160. [[CrossRef](#)] [[PubMed](#)]
55. Habibi, D.; Faraji, A.R.; Arshadi, M.; Veisi, H.; Gil, A. Manganese nanocatalyst and N-hydroxyphthalimide as an efficient catalytic system for selective oxidation of ethylbenzene, cyclohexene and oximes under aerobic condition. *J. Mol. Catal. A Chem.* **2014**, *382*, 41–54. [[CrossRef](#)]
56. Sapir, L.; Stanley, C.B.; Harries, D. Properties of Polyvinylpyrrolidone in a Deep Eutectic Solvent. *J. Phys. Chem. A* **2016**, *120*, 3253–3259. [[CrossRef](#)] [[PubMed](#)]
57. Prijic, S.; Sersa, G. Magnetic nanoparticles as targeted delivery systems in oncology. *Radiol. Oncol.* **2011**, *45*, 1–16. [[CrossRef](#)] [[PubMed](#)]
58. Balci, S.; Tomul, F. Catalytic wet peroxide oxidation of phenol through mesoporous silica-pillared clays supported iron and/or titanium incorporated catalysts. *J. Environ. Mana.* **2023**, *326 Pt B*, 116835. [[CrossRef](#)]
59. Huth, S.; Lausier, J.; Gersting, S.W.; Rudolph, C.; Plank, C.; Welsch, U.; Rosenecker, J. Insights into the mechanism of magnetofection using PEI-based magnetofectins for gene transfer. *J. Genet. Med.* **2004**, *6*, 923–936. [[CrossRef](#)] [[PubMed](#)]
60. Sassykova, L.; Kubekova, S.N.; Bатыrbayева, A.; Azhigulova, R.N.; Zhaxibayeva, Z.M.; Kozhaisakova, M.A.; Zhusupova, L.A.; Sendilvelan, S.; Ponomarenko, O. Hydrogenation of aromatic nitro compounds to amines on nickel and iron-containing catalysts. *Rasayan J. Chem.* **2021**, *14*, 1223–1229. [[CrossRef](#)]
61. Xenariou, S.; Griesenbach, U.; Ferrari, S.; Dean, P.; Scheule, R.K.; Cheng, S.H.; Geddes, D.M.; Plank, C.; Alton, E.W.F.W. Using magnetic forces to enhance non-viral gene transfer to airway epithelium in vivo. *Gene Ther.* **2006**, *13*, 1545–1552. [[CrossRef](#)]
62. Nakamoto, K. *Infrared and Raman Spectra of Inorganic and Coordination Compounds: Part A: Theory and Application in Inorganic Chemistry*; John Wiley & Sons: Hoboken, NJ, USA, 2008; pp. 240–295.

63. Petranovska, A.L.; Fedorenko, O.M.; Horbyk, P.P.; Chuyko, O.O.; Chehun, V.F.; Dubrovin, I.V.; Semko, L.S.; Storozhuk, L.P.; Abramov, M.V.; Revo, S.L. Development and properties of magnetically sensitive nanocomposites for directed transport of medicinal products. *Nanosistemi Nanomater. Nanotehnol.* **2005**, *3*, 812–823.
64. Ryberg, R. Infrared spectroscopy of adsorbed molecules: Some experimental aspects. *Le J. de Phys. Colloq.* **1983**, *44*, C10-421–C10-427. [[CrossRef](#)]
65. Semko, L.S.; Storozhuk, L.P.; Khutornoi, S.V.; Abramov, N.V.; Gorbik, P.P. Template synthesis, structure, and properties of magnetically controlled, large surface area Fe₃O₄/TiO₂ adsorbents. *Inorg. Mater.* **2015**, *51*, 430–435. [[CrossRef](#)]
66. Paukshtis, E.A.; Yurchenko, E.N. Study of the Acid–Base Properties of Heterogeneous Catalysts by Infrared Spectroscopy. *Russ. Chem. Rev.* **1983**, *52*, 242–258. [[CrossRef](#)]
67. Tsyganenko, A.A.; Smirnov, K.S.; Rzhhevskij, A.M.; Mardilovich, P.P. Infrared spectroscopic evidence for the structural OH groups of spinel alumina modifications. *Mater. Chem. Phys.* **1990**, *26*, 35–46. [[CrossRef](#)]
68. Davydov, A. *Molecular Spectroscopy of Oxide Catalyst Surfaces*; John Wiley & Sons: Hoboken, NJ, USA, 2003; 690p, ISBN 978-0-471-98731-4.
69. Aluker, N.L.; Lavrentieva, A.L.; Suzdaltseva, Y.M. Direct optical research methods in the analytics of phenol. *Opt. Spectrosc.* **2020**, *128*, 422–428. [[CrossRef](#)]
70. Lázár, K.; Nimz, M.; Lietz, G.; Guzzi, L. Formation of PdFe alloys on silica supported catalysts. *Hyperfine Interact.* **1988**, *41*, 657–660. [[CrossRef](#)]

Disclaimer/Publisher’s Note: The statements, opinions and data contained in all publications are solely those of the individual author(s) and contributor(s) and not of MDPI and/or the editor(s). MDPI and/or the editor(s) disclaim responsibility for any injury to people or property resulting from any ideas, methods, instructions or products referred to in the content.